Open Access

Catalysis Research

LIDSEN Publishing Inc.

Original Research

Enhanced Degradation of Methylene Blue and Methyl Orange Dyes Using Fe_3O_4@N-MWCNT as a Peroxymonosulfate Activator

Maksut Samedinov [1, 2], Gulsin Arslan [1], Idris Sargin [1, *]

1. Department of Biochemistry, Faculty of Science, Selçuk University, 42075, Konya, Turkey; E-Mails: samedinovmaxut@gmail.com; 71arslan@gmail.com; idris.sargin@selcuk.edu.tr; ORCID: 0009-0005-6207-2100; 0000-0002-4836-8651; 0000-0003-3785-9575
2. Department of Chemistry, Faculty of Science, Selçuk University, 42075, Konya, Turkey

* **Correspondence:** Idris Sargin; E-Mail: idris.sargin@selcuk.edu.tr; ORCID: 0000-0003-3785-9575

Academic Editor: Narendra Kumar

Catalysis Research
2026, volume 6, issue 3
doi:10.21926/cr.2603009

Received: January 12, 2026
Accepted: July 28, 2026
Published: August 04, 2026

Abstract

Peroxymonosulfate decomposition is crucial for environmental remediation, especially in degrading organic pollutants. Peroxymonosulfate can be oxidized by transition metals, generating hydroxyl and sulfate radicals that degrade pollutants. In this study, a heterogeneous catalyst (Fe_3O_4@N-MWCNT, a composite of Fe_3O_4 with nitrogen-doped multi-walled carbon nanotubes) was prepared, characterized (FT-IR, TEM, XRD, DSC), and used as a peroxymonosulfate activator for the degradation of Methylene Blue and Methyl Orange dyes in aqueous media. The results indicated that Fe_3O_4@N-MWCNT could serve as an effective peroxymonosulfate activator, reducing degradation times from hours to seconds (Methylene Blue: >180 min. to 32 s; Methyl Orange: >20 min. to 6 s). Moreover, the Fe_3O_4@N-MWCNT catalyst maintained its activity over 5 cycles. This study demonstrated that Fe_3O_4@N-MWCNT can serve as a highly effective activator of peroxymonosulfate, thereby holding significant potential for remediating water sources contaminated with Methylene Blue and Methyl Orange dyes.

Keywords

Dye degradation; magnetite; multiwalled carbon nanotubes; heterogeneous catalyst; peroxymonosulfate decomposition

1. Introduction

Textile wastewater poses a significant challenge because of the complexity and often hazardous nature of the discharges generated during textile manufacturing [1]. One of the primary pollutants in textile wastewater is organic dyes, which are widely used in textile manufacturing. These dyes have highly stable chemical structures, which slow and inefficiently degrade in the environment [2, 3]. Because most dyes are water-soluble, they reduce light penetration in aquatic ecosystems, hindering photosynthesis and threatening aquatic biodiversity. This, in turn, increases oxygen demand, as reflected in elevated biochemical and chemical oxygen demand [4]. Even at low concentrations, they exert toxic, mutagenic, and carcinogenic effects and contribute to decreased dissolved oxygen levels [5]. Traditional water treatment methods for textiles often fall short because techniques such as membrane filtration, ozonation, adsorption, and coagulation don't effectively degrade dyes. That's why there's a need for a new, eco-friendly approach to remove organic dyes from water.

Methylene Blue (MB) is a common dye found in textile wastewater. It's a thiazine dye with the chemical formula $C_{16}H_{18}ClN_3S$ and can also exist as a hydrate, $C_{16}H_{18}ClN_3S{\cdot}H_2O$ [6]. Recent research indicates that at high concentrations, MB can interfere with oxygen uptake by hemoglobin, potentially leading to hypoxia [7]. At excessive doses, this dye can also raise methemoglobin levels, which hampers oxygen transport in the body [8]. Additionally, MB acts as a monoamine oxidase inhibitor (MAOI), affecting serotonin levels. When combined with other serotonergic agents, it may trigger serotonin syndrome, characterized by symptoms such as fever, sweating, confusion, tremors, and seizures [9]. Given the toxic effects of MB, exploring effective methods for treating wastewater containing MB is an important area of investigation.

In addition to MB, other dyes, such as Methyl Orange (MO), can also affect human health. MO is a synthetic acid-base indicator with the chemical formula $C_{14}H_{14}N_3NaO_3S$, used for pH testing and as a coloring agent in chemical and biological labs [10]. In textile wastewater, it is often used for purposes similar to MB. Although their applications overlap, it is important to note that MO can be equally toxic as MB even at lower concentrations [11].

Recent research shows that advanced oxidation methods, which use various reactive oxygen species (ROS) in chemical remediation, are effective at degrading dyes in water. Among these methods, sulfate radical-based processes are particularly powerful for degrading persistent organic pollutants in complex aqueous environments [12]. Potassium peroxymonosulfate ($KHSO_5$) is a typical persulfate salt with an asymmetric structure and is widely used to generate reactive oxygen species, such as sulfate and hydroxyl radicals, for further oxidation. Transition metals such as Fe, Co, and Mn, and their oxides, are excellent activators of peroxymonosulfates; they facilitate the formation of radical species ($SO_4^{\bullet-}$, $^{\bullet}OH$) [13, 14].

Studies in the literature on PMS activation indicate that activation occurs through conversion to active oxidant species. Possible reactions after activation are listed below.

1. $S_2O_8^{2-} \rightarrow 2SO_4^{\bullet-}$
2. $HSO_5^- \rightarrow SO_4^{\bullet-} + HO^{\bullet}$
3. $SO_4^{\bullet-} + H_2O \rightarrow SO_4^{2-} + HO^{\bullet} + H^+$

Literature reports that the high performance of Fe- and N-doped carbon-based catalysts in PMS activation stems from structural and electronic synergy. Nitrogen doping enhances the electron conductivity of the carbon and promotes the formation of graphitic N and Fe-N active sites, thereby facilitating PMS adsorption and activation. Meanwhile, iron species within the carbon matrix accelerate electron transfer and the Fe^{3+}/Fe^{2+} redox cycle, supporting both radical and non-radical mechanisms. This synergistic effect significantly enhances catalytic activity and PMS activation efficiency [15-17].

When exposed to oxidizing agents or other aggressive species in aqueous solutions, MO can initiate radical attacks on azo compounds, leading to toxic effects. The literature confirms that breaking the azo bond in the MO molecule can release aniline derivatives, which are known for their toxicity and carcinogenicity [18].

Advanced oxidation processes (AOPs) that combine peroxymonosulfate (PMS) with various catalysts or under different conditions have attracted significant attention for their efficacy in degrading persistent organic pollutants. For instance, when PMS is used with activated carbon fibers, it greatly enhances the breakdown of these pollutants, resulting in high removal efficiencies [19]. This highlights the potential of combining diverse materials and methodologies to enhance PMS activation for environmental applications.

This study involves the preparation of a heterogeneous catalyst (Fe_3O_4@N-MWCNT). This catalyst activates peroxymonosulfate to degrade MB and MO dyes in an aqueous solution. MB and MO dyes were chosen as model compounds to evaluate the effectiveness of the synthesized catalyst in dye degradation. The novelty of this work lies in the design and synthesis of a magnetically recoverable Fe_3O_4@N-MWCNT nanocomposite, where the synergistic interaction between Fe_3O_4 nanoparticles and N-MWCNTs enhances catalytic performance.

2. Experimental

2.1 Materials

Iron(III) chloride hexahydrate ($FeCl_3 \cdot 6H_2O$), iron(II) chloride tetrahydrate ($FeCl_2 \cdot 4H_2O$), hydrochloric acid (HCl), nitric acid (HNO_3), ethanol (C_2H_5OH), urea (NH_2CONH_2), methylene blue ($C_{16}H_{18}ClN_3S$), and methyl orange ($C_{14}H_{14}N_3NaO_3S$) were obtained from Merck. Potassium peroxymonosulfate (PMS) and ammonia solution ($NH_3 \cdot H_2O$) were obtained from Sigma-Aldrich. Aldrich supplied multi-walled carbon nanotubes (MWCNT).

2.2 Synthesis of the Catalysts

Three types of carbon-based catalysts, known as carbocatalysts, were produced: N-MWCNT, Fe_3O_4@MWCNT, and Fe_3O_4@N-MWCNT (Figure 1). In brief, MWCNTs were processed in a highly acidic environment to create functionalized MWCNTs, specifically in a carboxylated/hydroxylated form. Following this, the functionalized MWCNT was treated with an alkaline solution of Fe^{2+}/Fe^{3+} to yield Fe_3O_4@MWCNT, or it was reacted with urea to produce N-doped MWCNT (N-MWCNT).

Subsequently, N-MWCNT underwent treatment in an alkaline solution of Fe^{2+}/Fe^{3+} to generate Fe_3O_4@N-MWCNT. Further details are provided below.

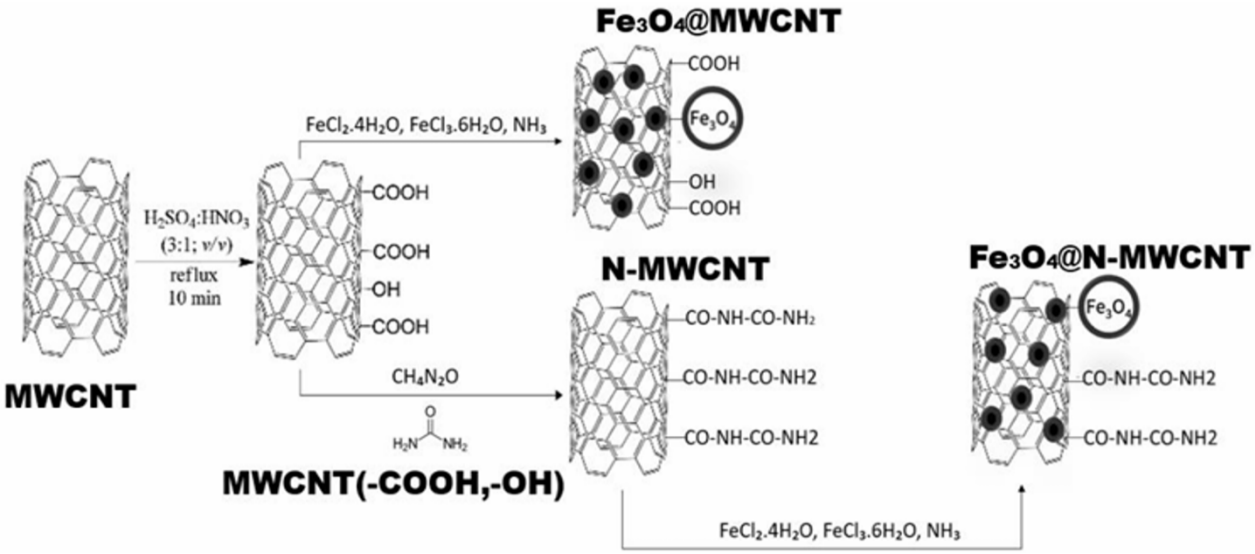

Figure 1 The steps for the synthesis of the catalysts.

2.2.1 Preparation of Functionalized MWCNTs

1.0 g of MWCNTs was treated in a strongly acidic medium (1:3 molar ratio of hydrochloric acid and nitric acid) at 60°C for 12 h under magnetic stirring. After treatment, MWCNTs were washed several times with ethanol and distilled water and dried in an oven at 80°C for 4 h. This process led to the formation of carboxyl and hydroxyl groups on the surface of carbon nanotubes. After the drying was complete, it was observed that MWCNTs exhibited hygroscopic properties, so the drying was performed in a lyophilizer. The carboxyl groups formed facilitated the binding of magnetite (Fe_3O_4) particles and N-doping of the carbon nanotubes with urea (vide infra).

2.2.2 Synthesis of N-MWCNT

0.5 g of carboxylated MWCNT was thoroughly mixed with 1.5 g of urea. To this mixture, 50 mL of ultrapure water was added, and the solution was sonicated for 4 h to achieve a uniform structure. After sonication, the mixture was washed with ethanol to remove impurities, and the remaining liquid was lyophilized. This process enabled chemical modifications of the MWCNT surface, resulting in N-doping.

2.2.3 Synthesis of Fe_3O_4@MWCNT

1.0 g of carboxylated MWCNT was added to 100 mL of pure water to form a dispersion. Next, 0.225 g of $FeCl_2{\cdot}4H_2O$ was added, and the mixture was stirred at 70°C for 1 h. At the end of this period, 0.375 g of $FeCl_3{\cdot}6H_2O$ was added, and stirring continued for another 1 h at the same temperature. Then, 4.0 mL of NH_3 solution was added, and the reaction medium was stirred for 1 h. Finally, MWCNT loaded with magnetic particles (Fe_3O_4@MWCNT) was filtered and washed with water. The Fe_3O_4@MWCNT was dried in an oven at 80°C for 5 h and subsequently lyophilized. After drying, the magnetic properties were assessed.

2.2.4 Synthesis of Fe_3O_4@N-MWCNT

A dispersion was formed by adding 0.5 g of N-MWCNT to 50 mL of pure water. Then, 0.113 g of $FeCl_2 \cdot 4H_2O$ was introduced into this dispersion, and the mixture was stirred at 70°C for 1 h. After stirring, 0.186 g of $FeCl_3 \cdot 6H_2O$ was added, and the mixture was stirred for another hour at the same temperature. Next, 2.0 mL of NH_3 solution was added to the mixture, and the mixture was stirred for an additional hour. Following this, N-MWCNTs loaded with magnetic particles (Fe_3O_4@N-MWCNT) were filtered, washed with water, and dried in an oven at 80°C for 5 h. After drying, the samples were lyophilized. The magnetic properties of the resulting magnetic N-MWCNTs were then evaluated.

2.3 Instrumentation and Characterization

The FT-IR spectra of Fe_3O_4@N-MWCNT were recorded using a Bruker Vertex 70 FTIR spectrometer within the range of 4000–500 cm^{-1} to identify the functional groups on the catalyst surface. This analysis was performed to confirm the presence of imine and amino groups after N-doping. Additionally, the interaction between MWCNT and Fe_3O_4 nanoparticles was examined through characteristic spectral peaks. The crystalline phases of Fe_3O_4@N-MWCNT were investigated using X-ray diffraction (XRD). The analysis provided insights into the crystallinity and graphitic nature of MWCNT and the distinct crystalline structures of Fe_3O_4 (magnetite) nanoparticles. Transmission Electron Microscopy (TEM) was used to examine the catalyst's nanoscale morphology, size, and distribution. The images revealed uniform attachment of Fe_3O_4 nanoparticles to the MWCNT surface, highlighting the homogeneity of the composite. Differential Scanning Calorimetry (DSC) was performed to evaluate the thermal stability of Fe_3O_4@N-MWCNT. This technique provided information on the thermal resistance and chemical stability of the catalyst under varying temperature conditions, enabling the determination of optimal operating conditions.

2.4 Degradation of MB and MO Dyes

MB and MO stock solutions were prepared by dissolving certain amounts of the dyes in distilled water to give a final concentration of 1.0×10^{-4} M. In the degradation studies, MB and MO solutions were mixed with the Fe_3O_4@N-MWCNT catalyst, and degradation was initiated by the addition of PMS. Once the characteristic color of the dyes disappeared, the clear solution was immediately pipetted into a quartz cuvette and monitored using a UV-vis spectrophotometer at the specific absorbance for each degradation experiment. In the case of MB, the degradation was evidenced by the disappearance of the peak at 664 nm, whereas for MO, it was shown by the absence of the peak at 464 nm. Additionally, methanol (15% v/v) was added as a radical scavenger to effectively quench sulfate and hydroxyl radicals, although it did not fully deactivate PMS.

In the study, a heterogeneous Fe_3O_4@N-MWCNT catalyst was used, which was quickly separated by magnetic filtration before quenching to prevent further PMS activation and oxidation. Reaction conditions and reusability tests for the Fe_3O_4@N-MWCNT catalyst are detailed in Table 1, Table 2, and Table 3. The temperature of the reaction vessel was maintained with a water bath during temperature studies.

Table 1 The catalytic activity of the functionalized MWCNT, N-MWCNT, Fe_3O_4@MWCNT, and Fe_3O_4@N-MWCNT in the degradation of MB dye (pH 8.0).

Batch (variable)	MB volume (mL)	Catalyst (mg)	C_{PMS} (mM)	Temperature (°C)	Time
1 (catalyst type)	1.0	1 mg MWCNT	8.45	21	1 min 24 s
	1.0	1 mg N-MWCNT	8.45	21	1 min 32 s
	1.0	1 mg Fe_3O_4@MWCNT	8.45	21	3 min
	1.0	1 mg Fe_3O_4@N-MWCNT	8.45	21	48 s
2* (C_{PMS})	1.0	1	8.45	21	48 s
	1.0	1	4.23	21	1 min 47 s
	1.0	1	2.11	21	3 min 12 s
	1.0	1	1.06	21	~10 min
3* (catalyst amount)	1.0	1	8.45	21	48 s
	1.0	2	8.45	21	45 s
	1.0	3	8.45	21	32 s
	1.0	5	8.45	21	32 s
4* (MB volume)	0.5	1	8.45	21	32 s
	1.0	1	8.45	21	38 s
	1.5	1	8.45	21	48 s
	2.0	1	8.45	21	5 min
	3.0	1	8.45	21	6 min 12 s
5* (temperature)	1.0	3	8.45	10	1 min 6 s
	1.0	3	8.45	21	32 s
	1.0	3	8.45	40	21 s

* The catalyst is Fe_3O_4@N-MWCNT.

Table 2 The catalytic activity of the functionalized MWCNT, N-MWCNT, Fe_3O_4@MWCNT, and Fe_3O_4@N-MWCNT in the degradation of MO dye (pH 7.4).

Batch	MO Volume (mL)	Catalyst (mg)	C_{PMS} (mM)	Temperature (°C)	Time
1 (catalyst type)	1.0	1 mg MWCNT	8.45	21	1 min 27 s
	1.0	1 mg N-MWCNT	8.45	21	1 min 7 s
	1.0	1 mg Fe_3O_4@MWCNT	8.45	21	1 min 9 s
	1.0	1 mg Fe_3O_4@N-MWCNT	8.45	21	1 min 3 s
2* (C_{PMS})	1.0	1	8.45	21	1 min 3 s
	1.0	1	4.23	21	42 s
	1.0	1	2.11	21	1 min 20 s
	1.0	1	1.06	21	1 min 31 s
3* (catalyst amount)	1.0	1	4.23	21	32 s
	1.0	2	4.23	21	9 s
	1.0	3	4.23	21	6 s
4* (MO volume)	1.0	3	4.23	21	6 s
	2.0	3	4.23	21	48 s
	3.0	3	4.23	21	1 min 2 s
5* (temperature)	1.0	3	4.23	10	1 min 14 s
	1.0	3	4.23	21	6 s
	1.0	3	4.23	40	4 s

* The catalyst is Fe_3O_4@N-MWCNT.

Table 3 The reaction times that were recorded after the Fe_3O_4@N-MWCNT catalyst was reused in the degradation of the MB and MO (1.0 mL dye solution, 3 mg Fe_3O_4@N-MWCNT, C_{PMS}: 8.45 mM (MB) and 4.23 mM (MO), 21°C).

Dye	Number of cycles	Degradation time
MB	1st	32 s
	2nd	38 s
	3rd	56 s
	4th	1 min 24 s
	5th	1 min 45 s
MO	1st	6 s
	2nd	36 s
	3rd	1 min 01 s
	4th	1 min 55 s
	5th	3 min 27 s

2.4.1 Reusability Tests

In reusability tests, the Fe_3O_4@N-MWCNT catalyst was recovered using a magnet, washed with distilled water, dried, and reused in the degradation of MB or MO to demonstrate the catalyst's stability and reusability over multiple cycles (5 cycles).

2.4.2 Degradation of MB and MO Dyes Without PMS Activator

The degradation of MB and MO dyes without a PMS activator (i.e., Fe_3O_4@N-MWCNT) was studied under optimal conditions (i.e., the entries that yielded the shortest degradation times in Table 1 and Table 2). The degradation process was monitored spectrophotometrically.

3. Results and Discussion

3.1 Characterization of Fe_3O_4@N-MWCNT Catalyst

3.1.1 TEM Analysis

TEM analysis was conducted to examine the size and morphology of the Fe_3O_4@N-MWCNT catalyst. TEM analysis showed that the Fe_3O_4 nanoparticles were mostly spherical, but their distribution in the N-MWCNT matrix was uneven. Some aggregation of the nanoparticles was observed, likely due to magnetic interactions between the Fe_3O_4 particles and variations in surface defects and topography of the MWCNT. This uneven distribution could affect the catalytic properties of the composite, resulting in localized areas with higher activity (Figure 2).

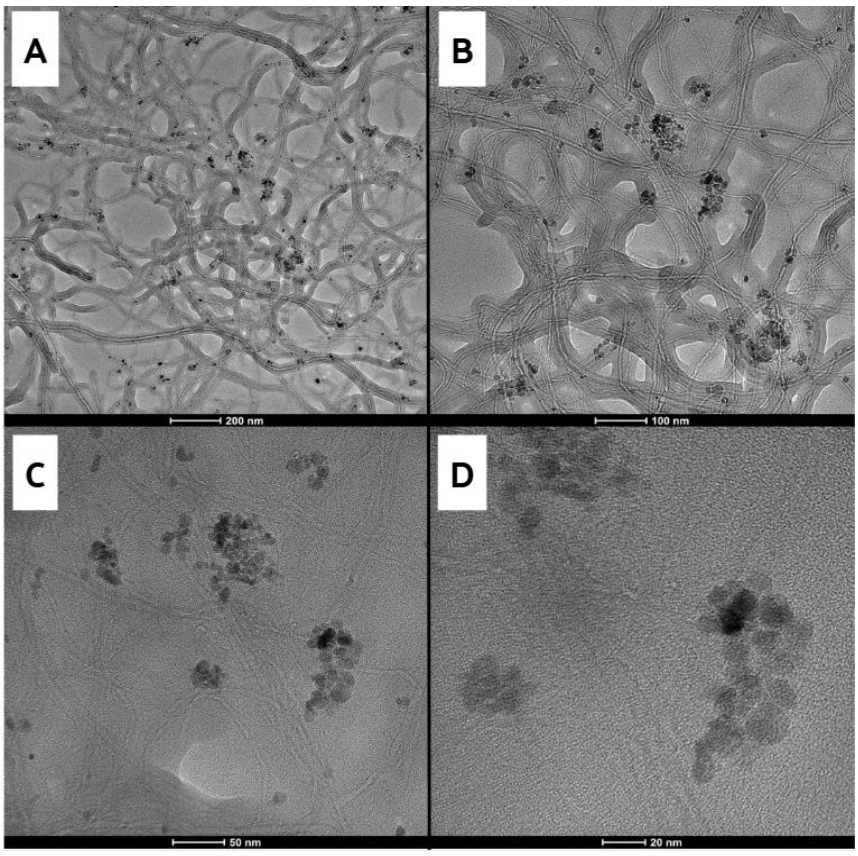

Figure 2 TEM images of Fe_3O_4@N-MWCNT (scale bars: A: 200 nm, B: 100 nm, C: 50 nm, and D: 20 nm).

The fibrous network in TEM images (Figures 2A, 2B) is attributed to N-MWCNT, which serves as a conductive and structurally supportive framework [20]. The dark, agglomerated regions dispersed along the nanotubes correspond to Fe_3O_4 nanoparticles affixed to the N-MWCNT surface via

electrostatic interactions and functionalization. Higher magnification TEM images (Figures 2C, 2D) further reveal the morphology of the Fe_3O_4 nanoparticles, showing their tendency to cluster while maintaining a nanoscale dispersion [21]. The nanoparticle size remains consistent at roughly 20 nm in diameter, indicating controlled synthesis and uniform dispersion [22].

3.2 FT-IR Spectroscopy Analysis of Fe_3O_4@N-MWCNT

Figure 3, Figure 4, and Figure 5 present the FT-IR spectra of the catalysts, which were analyzed to identify the organic functional groups present in the catalysts. FT-IR spectroscopy was used to identify the functional groups responsible for the catalytic degradation of dyes. The results highlight chemical interactions and confirm the successful formation of the catalyst, which played a key role in dye-degradation processes as follows [23-25]: The FT-IR spectra comparison between pristine MWCNT and acidified MWCNT shows notable differences due to surface modification. The peak around 1660 cm^{-1} in the carboxylated MWCNT spectrum corresponds to the C=O stretch of carboxyl groups, indicating successful functionalization. Additionally, the broad band between 2750–3500 cm^{-1} is attributed to O–H stretching from the carboxyl groups and adsorbed water. The bands at 1103, 1005, 869, and 542 cm^{-1} in the fingerprint region reflect the nanotube structure and modifications from oxygenated groups. Conversely, weaker, less-defined bands in these regions for pure MWCNT suggest fewer oxygen functional groups. Overall, FT-IR results confirm effective carboxylation and surface functionalization of MWCNT with oxygen-containing groups.

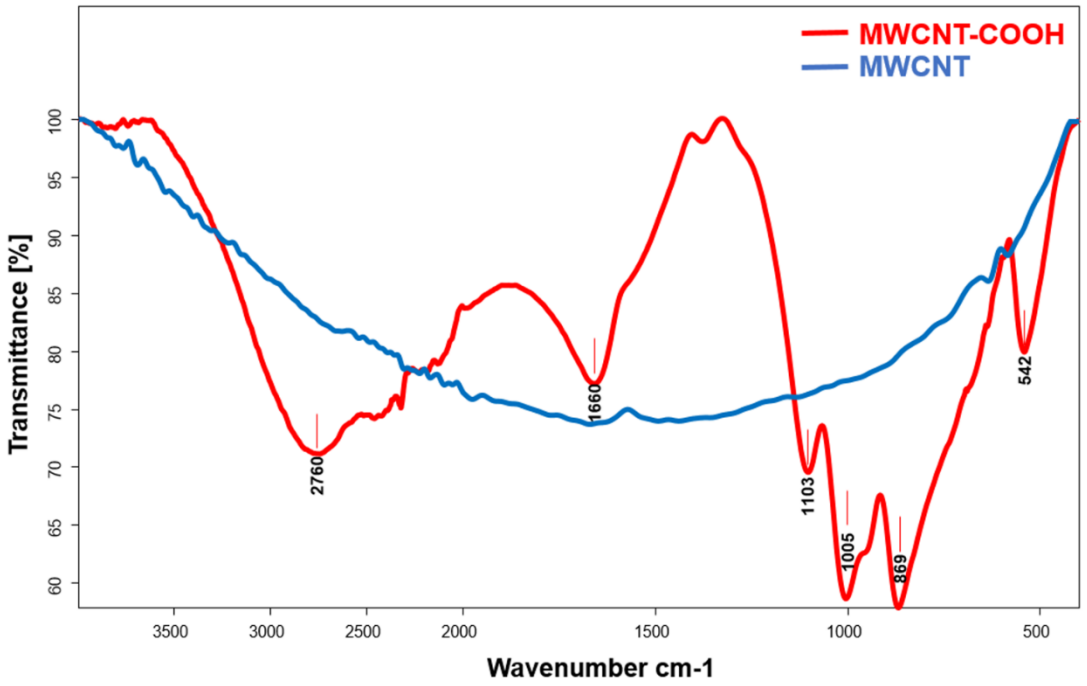

Figure 3 FT-IR spectra of carboxylated MWCNT (MWCNT-COOH) and pristine MWCNT.

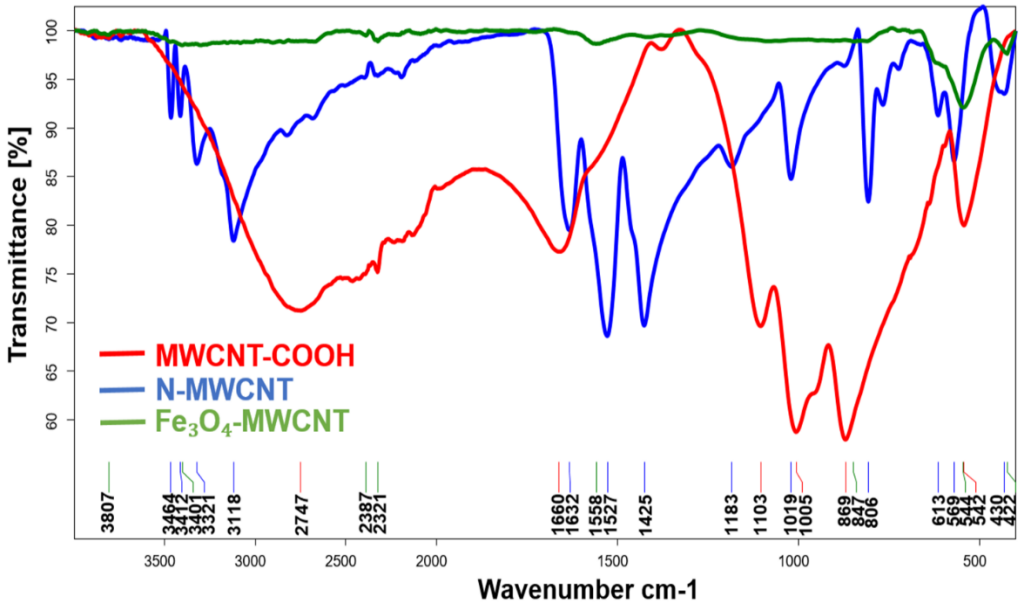

Figure 4 FT-IR spectra of carboxylated MWCNT (MWCNT-COOH), nitrogen-doped MWCNT (N-MWCNT), and magnetite-loaded MWCNT (Fe_3O_4-MWCNT).

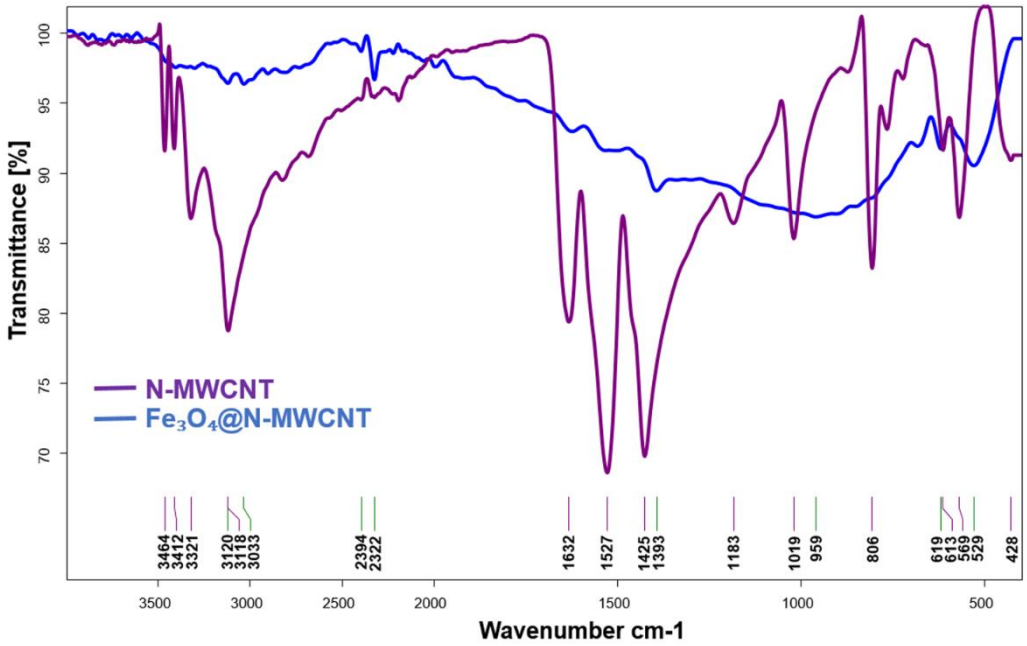

Figure 5 FT-IR spectra of magnetite-loaded N-MWCNT (Fe_3O_4@N-MWCNT) and nitrogen-doped MWCNT (N-MWCNT).

Analyzing the FT-IR spectra of MWCNT-COOH, N-MWCNT, and Fe_3O_4-MWCNT samples highlights the emergence of distinct vibrational bands at each stage of modification. The broad absorption around 3400 cm^{-1} in N-MWCNT spectra corresponds to N–H stretching vibrations. Additionally, bands between 1558–1527 cm^{-1} indicate successful nitrogen incorporation and the formation of nitrogenous groups. For Fe_3O_4-MWCNT, notable bands in the 500–600 cm^{-1} range are observed, particularly around 544 cm^{-1} and 422 cm^{-1}, which are associated with Fe_3O_4 stretching vibrations and confirm the attachment of Fe_3O_4 nanoparticles. These bands serve as characteristic FT-IR

signatures of spinel-structured iron oxides. Overall, the spectral data confirm the successful nitrogen doping and Fe_3O_4 loading processes at each modification step.

Comparing the FT-IR spectra of N-MWCNT and Fe_3O_4@N-MWCNT samples reveals characteristic spectral changes due to the successful loading of Fe_3O_4 nanoparticles onto the nitrogen-doped carbon nanotube surface. In the spectrum of the Fe_3O_4@N-MWCNT composite, new and broad absorption bands, particularly in the 500–600 cm^{-1} range, are noteworthy. These bands correspond to Fe–O stretching vibrations and confirm the successful immobilization of Fe_3O_4 nanoparticles onto the carbon nanotube surface. Furthermore, the decrease in intensity or broadening of some sharp bands observed in the N-MWCNT spectrum and their absence in the Fe_3O_4@N-MWCNT spectrum indicate the formation of strong interactions between Fe_3O_4 nanoparticles and the nitrogen-doped carbon nanotube surface, suggesting a change in the chemical environment of the surface. These findings provide significant characterization evidence demonstrating the successful structural achievement of the synthesized Fe_3O_4@N-MWCNT composite.

3.3 XRD Analysis of Fe_3O_4@N-MWCNT

The XRD pattern shows distinct peaks at 2θ values of around 26° and 44° (Figure 6). These peaks correspond to the (002) and (100) planes of N-MWCNT, respectively, confirming the presence of carbon nanotubes. Additionally, other peaks at approximately 18°, 30°, 35.5°, 53°, 57°, 62.5°, and 74.5° in 2θ indicate Bragg reflections from the (111), (220), (311), (422), (511), (440), and (533) planes of Fe_3O_4 [26]. These characteristic peaks confirm the presence of the spinel crystal structure of Fe_3O_4, indicating the successful synthesis of the nanocomposite. The XRD analysis also demonstrates that the nanocomposite possesses a well-defined and highly ordered crystalline structure, confirming its crystalline nature rather than an amorphous phase [27].

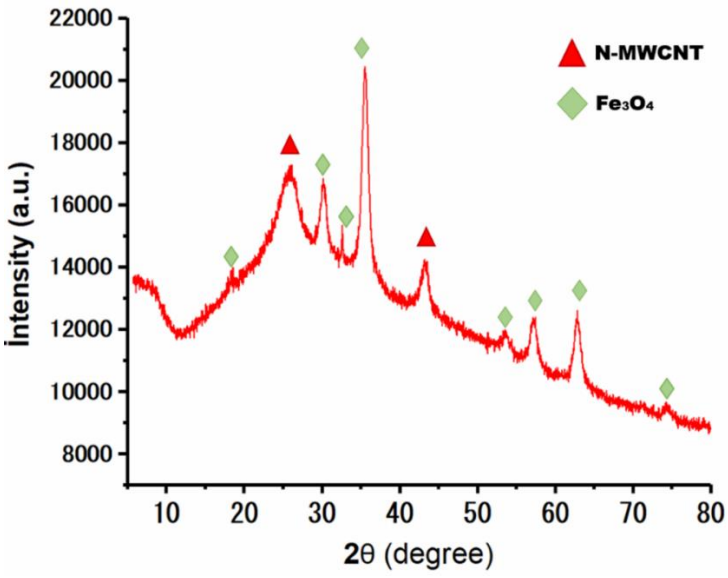

Figure 6 XRD pattern of Fe_3O_4@N-MWCNT.

3.4 DSC Analysis of Fe_3O_4@N-MWCNT

In the DSC analysis (Figure 7), a distinct endothermic event was observed, starting at 137.96°C, peaking at 161.39°C, and ending at 178.29°C. This sharp endothermic peak indicates the material's

melting and a significant structural change. The enthalpy change, calculated from the peak area, was -13.83 mJ, corresponding to a normalized value of -7.68 J/g, indicating a substantial amount of energy required for the phase transition. These results strongly suggest a well-defined thermal response, confirming the material's structural stability and phase behavior under thermal stress [28].

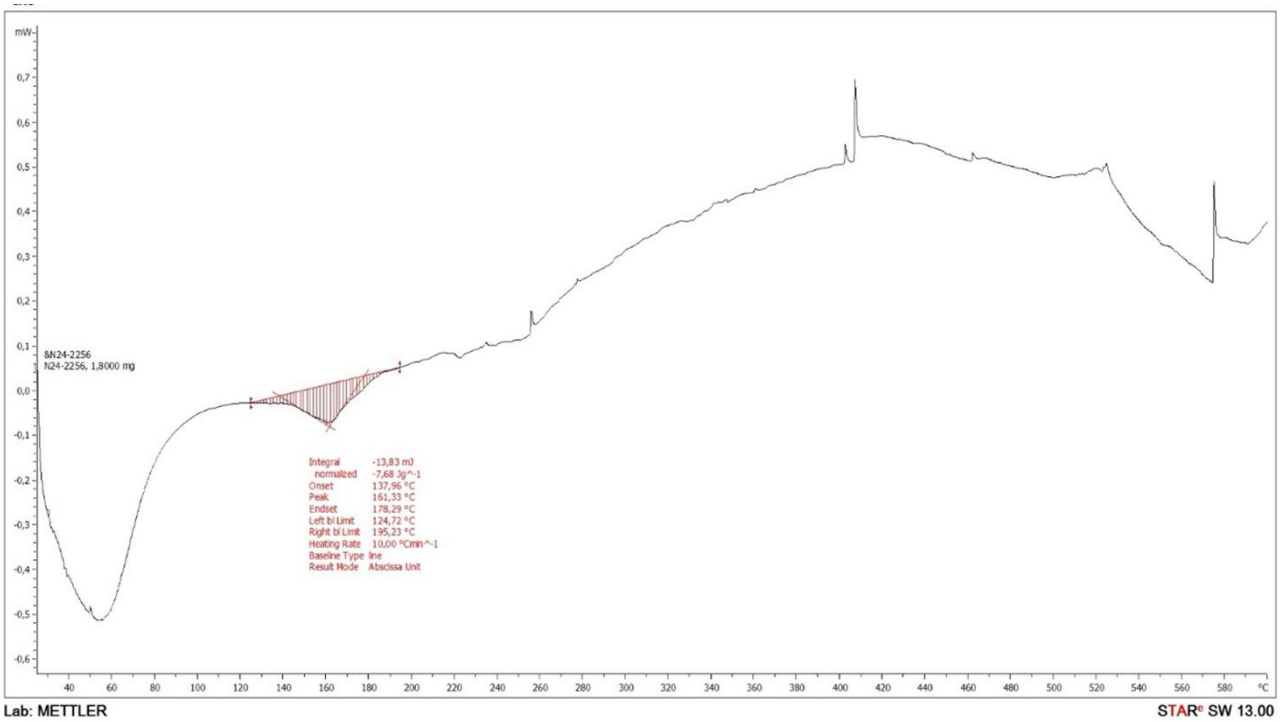

Figure 7 DSC analysis of Fe_3O_4@N-MWCNT.

3.5 Catalytic Activity of Fe_3O_4@N-MWCNT in the Degradation of Dyes

Conventional oxidation and adsorption techniques often have limited efficiency, high operating costs, and cause secondary pollution. Therefore, creating multifunctional nanocomposites that can efficiently activate peroxymonosulfate (PMS) to generate reactive oxygen species under mild conditions has become a key research area.

The catalytic activity of the functionalized MWCNT, N-MWCNT, Fe_3O_4@MWCNT, and Fe_3O_4@N-MWCNT in the degradation of MO and MB dyes is shown in Table 1 and Table 2. The results presented in Table 1 and Table 2 demonstrate that Fe_3O_4@N-MWCNT is a superior peroxymonosulfate activator for the degradation of MB and MO dyes in aqueous media. This observation also demonstrates the effects of N doping. Compared to Fe_3O_4@N-MWCNT, Fe_3O_4@MWCNT was significantly less effective as a peroxymonosulfate activator in degrading MB and MO dyes. As presented in Table 3, Fe_3O_4@N-MWCNT maintained its activity over 5 cycles, demonstrating its reusability in environmental applications and remediation. Additionally, the catalyst was easily recovered from the medium with a magnet, another advantage.

In chemical remediation technology, advanced oxidation processes (AOPs) have recently been reported to effectively degrade plastic pollutants in water through various reactive oxygen species (ROS) [29]. Among these processes, sulfate radical ($SO_4^{\bullet-}$)–based methods stand out as highly effective for degrading recalcitrant organic pollutants in complex water matrices [12]. Peroxymonosulfate ($HO\text{-}SO_4^-$), an asymmetric persulfate salt, is commonly used in advanced

oxidation processes to generate highly reactive oxygen species, such as $SO_4^{\bullet-}$ and $HO^{\bullet}$ radicals [30]. Transition metals (e.g., Fe, Co, Mn) and their oxides serve as excellent catalysts for activating peroxymonosulfate, promoting the formation of $SO_4^{\bullet-}$ and $HO^{\bullet}$ species [13]. Doping heteroatoms such as B, N, S, and P into the sp^2 carbon lattice of carbon nanotubes can enhance the catalytic efficiency of the active sites for peroxymonosulfate activation [31]. Consequently, heteroatom-doped carbon nanotubes and transition-metal-based catalysts are promising materials for the effective breakdown of environmental pollutants.

Magnetite nanoparticles have excellent magnetic and electrical properties that facilitate electron transfer between ferrous and ferric ions. They activate O–O bonds in persulfate, hydrogen peroxide, and PMS, generating reactive oxygen species [32]. Oxidant molecules adsorb onto magnetite particles, and ferrous ions in nanoparticles donate electrons, generating radicals such as superoxide, hydroperoxyl, and sulfate radicals [33].

As presented in Table 1 and Table 2, with a constant catalyst dosage, the catalytic performance of the synthesized Fe_3O_4@N-MWCNT composite was systematically evaluated for MB degradation via PMS activation. Comparative studies confirmed that the synergistic interaction between the nitrogen-doped carbon framework and the encapsulated iron species enabled ultra-fast degradation. Optimization of operational parameters further demonstrated that increasing catalyst loading to 3 mg accelerated radical generation, reducing reaction time to 32 s by maximizing active site density. Moreover, the system exhibited remarkable robustness across varying pollutant loads. It achieved complete degradation within 21 s at 40°C, underscoring its high thermal sensitivity and potential for efficient, large-scale water treatment applications. The catalytic performance of the Fe_3O_4@N-MWCNT composite was further confirmed using MO as a model pollutant. The composite exhibited superior activity compared with pristine and control samples, achieving complete MO degradation within 63 s. Optimization studies revealed that increasing catalyst dosage significantly enhanced reaction kinetics, reducing the degradation time to 6 s at 3 mg catalyst loading. Moreover, the system maintained excellent performance across varying pollutant loads and elevated temperatures, demonstrating the potential of Fe_3O_4@N-MWCNT as an efficient PMS activator for advanced oxidative water treatment.

The reusability tests revealed that the catalytic activity of Fe_3O_4@N-MWCNT started to decline, especially after the third cycle (Table 3). This decrease may be due to the catalyst loss during recovery. However, the catalyst still performed well even after the fifth cycle.

3.6 Degradation of MB and MO Dyes without PMS Activator

The degradation of MB and MO dyes was investigated in the absence of a PMS activator (i.e., Fe_3O_4@N-MWCNT) under optimal conditions (please refer to the best degradation times in Table 1 and Table 2). The process was monitored using UV-vis spectrophotometry (Figure 8). The degradation of MO dye took 20 min, whereas the degradation of MB dye required up to 180 min. These findings indicate that a PMS activator, such as Fe_3O_4@N-MWCNT, is necessary to achieve effective results when using PMS as a radical source. Previous studies confirm that while PMS is a thermodynamic oxidant, its direct reaction with most contaminants is impractical. Thus, a catalyst activation is necessary [34, 35]. Table 4 summarizes recent studies on the activation of peroxymonosulfate for pollutant degradation.

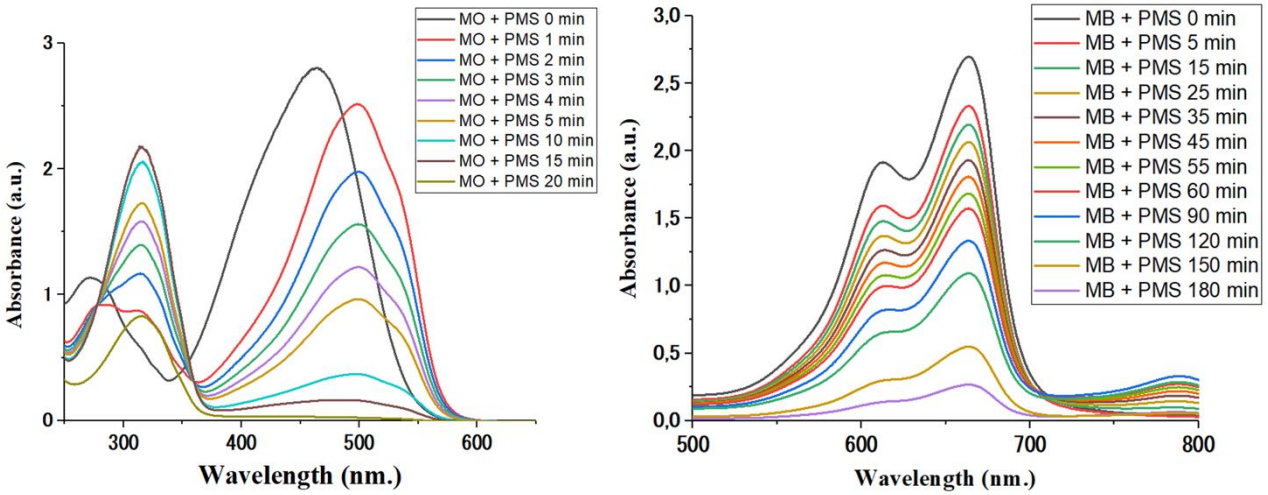

Figure 8 The degradation of MO and MB dyes in the absence of the PMS activator (i.e., Fe_3O_4@N-MWCNT) under optimal conditions.

Table 4 Comparison of recently published studies on peroxymonosulfate activation for pollutant degradation.

Year	Reference	PMS Activator	Results
2024	[36]	Fe_3O_4@GO	Degradation efficiency of Rhodamine B (RhB) was significantly increased to a level of ≈95%.
2025	[37]	$Sn_{0.96}Ni_{0.02}Co_{0.02}$/Al/Ce/ Mo type-II oxide heterojunction	RSM-CCD optimized photo-Fenton-like process under visible light conditions.
2025	[38]	$Sn_{0.96}$-$Fe_{0.02}$-$Ni_{0.02}$/Al-Ce-Mo oxide heterojunction	98.31% phenol removal in 90 min via PMS-activated photo-Fenton process.
2026	[39]	$Zn_{0.98}Co_{0.02}O$/GGAC/γ-Al_2O_3/ CeO_2/α-MoO_3 heterojunction	Achieved 97.81% removal of 17α-ethinylestradiol (EE2) via synergistic PMS and visible-light activation.
2026	This work	Fe_3O_4@N-MWCNT	Please refer to the text.

4. Conclusion

This study revealed that (i) peroxymonosulfate decomposition, which generates radical species such as $SO4^{\bullet-}$ and $HO^{\bullet}$, has significant potential for treating water contaminated with Methylene Blue and Methyl Orange dyes. (ii) Peroxymonosulfate decomposition requires activation by a catalyst containing a transition metal. (iii) Magnetite (Fe_3O_4), a double oxide, is an effective activator of peroxymonosulfate. (iv) N-doping of MWCNT is necessary to enhance the catalytic performance of the Fe_3O_4@N-MWCNT catalyst system. (v) Fe_3O_4@N-MWCNT can maintain its activity over five cycles. The study also found that N-doping of MWCNT influences the catalytic activity of the Fe_3O_4@N-MWCNT system during peroxymonosulfate decomposition. Fe_3O_4@N-MWCNT appears promising for water treatment, especially for removing Methylene Blue and Methyl Orange from aqueous media. It acts as an efficient, magnetically recoverable peroxymonosulfate activator, achieving dye degradation in seconds and retaining activity over five reuse cycles. However, the

Fe_3O_4@N-MWCNT catalyst system should be tested in a pilot system. This should be explored further in future studies.

Author Contributions

Maksut Samedinov: Conceptualization, Formal analysis, Investigation, Methodology, Visualization, Writing – original draft. Idris Sargin: Supervision, Writing – original draft, Writing – review & editing. Gulsin Arslan: Conceptualization, Supervision, Writing – review & editing.

Funding

This study was partially funded by TUBITAK 2209-A program (Grant no: 1919B012301017).

Competing Interests

The authors have declared that no competing interests exist.

AI-Assisted Technologies Statement

Artificial intelligence (AI) tools were used solely for basic grammar correction and language refinement in the preparation of this manuscript. Specifically, Grammarly (which tools were used) was employed to improve the readability and linguistic clarity of the English text. All scientific content, data interpretation, and conclusions were developed independently by the author. The authors have thoroughly reviewed and edited the AI-assisted text to ensure its accuracy and accept full responsibility for the content of the manuscript.

References

1. Kallawar GA, Bhanvase BA. A review on existing and emerging approaches for textile wastewater treatments: Challenges and future perspectives. Environ Sci Pollut Res. 2024; 31: 1748-1789.
2. Islam T, Repon MR, Islam T, Sarwar Z, Rahman MM. Impact of textile dyes on health and ecosystem: A review of structure, causes, and potential solutions. Environ Sci Pollut Res. 2023; 30: 9207-9242.
3. Hynes NR, Kumar JS, Kamyab H, Sujana JA, Al-Khashman OA, Kuslu Y, et al. Modern enabling techniques and adsorbents based dye removal with sustainability concerns in textile industrial sector-A comprehensive review. J Clean Prod. 2020; 272: 122636.
4. Mbachu CA, Babayemi AK, Egbosiuba TC, Ike JI, Ani IJ, Mustapha S. Green synthesis of iron oxide nanoparticles by Taguchi design of experiment method for effective adsorption of methylene blue and methyl orange from textile wastewater. Results Eng. 2023; 19: 101198.
5. Osorio-Aguilar DM, Saldarriaga-Noreña HA, Murillo-Tovar MA, Vergara-Sánchez J, Ramírez-Aparicio J, Magallón-Cacho L, et al. Adsorption and photocatalytic degradation of methylene blue in carbon nanotubes: A review with bibliometric analysis. Catalysts. 2023; 13: 1480.
6. Santoso E, Ediati R, Kusumawati Y, Bahruji H, Sulistiono DO, Prasetyoko D. Review on recent advances of carbon based adsorbent for methylene blue removal from waste water. Mater Today Chem. 2020; 16: 100233.

7. Ryou MG, Choudhury GR, Li W, Winters A, Yuan F, Liu R, et al. Methylene blue-induced neuronal protective mechanism against hypoxia-reoxygenation stress. Neuroscience. 2015; 301: 193-203.
8. Pushparajah Mak RS, Liebelt EL. Methylene blue: An antidote for methemoglobinemia and beyond. Pediatr Emerg Care. 2021; 37: 474-477.
9. Ng BK, Cameron AJ. The role of methylene blue in serotonin syndrome: A systematic review. Psychosomatics. 2010; 51: 194-200.
10. Iwuozor KO, Ighalo JO, Emenike EC, Ogunfowora LA, Igwegbe CA. Adsorption of methyl orange: A review on adsorbent performance. Curr Res Green Sustain Chem. 2021; 4: 100179.
11. Haque E, Jun JW, Jhung SH. Adsorptive removal of methyl orange and methylene blue from aqueous solution with a metal-organic framework material, iron terephthalate (MOF-235). J Hazard Mater. 2011; 185: 507-511.
12. Wang C, Kang J, Liang P, Zhang H, Sun H, Tadé MO, et al. Ferric carbide nanocrystals encapsulated in nitrogen-doped carbon nanotubes as an outstanding environmental catalyst. Environ Sci Nano. 2017; 4: 170-179.
13. Zhou D, Chen L, Li J, Wu F. Transition metal catalyzed sulfite auto-oxidation systems for oxidative decontamination in waters: A state-of-the-art minireview. Chem Eng J. 2018; 346: 726-738.
14. Zhou Y, Ogawa N, Lin JM. Enhanced chemiluminescence of peroxomonosulfate-cobalt (II) system in the presence of dicarboxylic acids. Luminescence. 2011; 26: 280-288.
15. Wang X, Yang Y, Zhang Y, Li Q, Gong M, Zhang R, et al. Facile synthesis and capacitance properties of N-doped porous carbon/iron oxide composites through the single-step pyrolysis of coal-based polyaniline. J Porous Mater. 2018; 25: 845-853.
16. Zeng T, Li S, Hua J, He Z, Zhang X, Feng H, et al. Synergistically enhancing Fenton-like degradation of organics by *in situ* transformation from Fe_3O_4 microspheres to mesoporous Fe, N-dual doped carbon. Sci Total Environ. 2018; 645: 550-559.
17. Ma W, Wang N, Du Y, Tong T, Zhang L, Lin KY, et al. One-step synthesis of novel Fe_3C@ nitrogen-doped carbon nanotubes/graphene nanosheets for catalytic degradation of bisphenol A in the presence of peroxymonosulfate. Chem Eng J. 2019; 356: 1022-1031.
18. Carreón T, Hein MJ, Viet SM, Hanley KW, Ruder AM, Ward EM. Increased bladder cancer risk among workers exposed to *o*-toluidine and aniline: A reanalysis. Occup Environ Med. 2010; 67: 348-350.
19. Huang Z, Bao H, Yao Y, Lu J, Lu W, Chen W. Key role of activated carbon fibers in enhanced decomposition of pollutants using heterogeneous cobalt/peroxymonosulfate system. J Chem Technol Biotechnol. 2016; 91: 1257-1265.
20. Hou CL, Li TH, Zhao TK, Liu HG, Liu LH, Zhang WJ. Electromagnetic wave absorbing properties of multi-wall carbon nanotube/Fe_3O_4 hybrid materials. New Carbon Mater. 2013; 28: 184-190.
21. Alkallas FH, Alghamdi SM, Rashed EA, Trabelsi AB, Nafee SS, Elsharkawy WB, et al. Nanocomposite Fe_3O_4-MWCNTs based on femtosecond pulsed laser ablation for catalytic degradation. Diamond Relat Mater. 2023; 140: 110445.
22. Folsom SK, Ivey DJ, McNair FS, Siamaki AR. Nickel-Fe_3O_4 magnetic nanoparticles supported on multiwalled carbon nanotubes: Effective catalyst in Suzuki cross coupling reactions. Catalysts. 2021; 11: 495.
23. Misra A, Tyagi PK, Rai P, Misra DS. FTIR spectroscopy of multiwalled carbon nanotubes: A simple approach to study the nitrogen doping. J Nanosci Nanotechnol. 2007; 7: 1820-1823.

24. Chauhan N, Pundir CS. An amperometric acetylcholinesterase sensor based on Fe_3O_4 nanoparticle/multi-walled carbon nanotube-modified ITO-coated glass plate for the detection of pesticides. Electrochim Acta. 2012; 67: 79-86.
25. Moghim MH, Zebarjad SM. Fabrication and structural characterization of multi-walled carbon nanotube/Fe_3O_4 nanocomposite. J Inorg Organomet Polym Mater. 2015; 25: 1260-1266.
26. Yuan H, Xu Y, Jia H, Zhou S. Superparamagnetic Fe_3O_4/MWCNTs heterostructures for high frequency microwave absorption. RSC Adv. 2016; 6: 67218-67225.
27. Liu Y, Wu N, Wang Z, Cao H, Liu J. Fe_3O_4 nanoparticles encapsulated in multi-walled carbon nanotubes possess superior lithium storage capability. New J Chem. 2017; 41: 6241-6250.
28. Liu S, Wang P, Yang Y, Yang Y, Wu G, Li H, et al. Influence of MWCNTs and nano-Fe_3O_4 on the properties and structure of MWCNTs/Fe_3O_4/PLA composite film with electromagnetic interference shielding function. J Polym Res. 2020; 27: 288.
29. Kang J, Zhou L, Duan X, Sun H, Ao Z, Wang S. Degradation of cosmetic microplastics via functionalized carbon nanosprings. Matter. 2019; 1: 745-758.
30. Wojnárovits L, Tóth T, Takács E. Critical evaluation of rate coefficients for hydroxyl radical reactions with antibiotics: A review. Crit Rev Environ Sci Technol. 2018; 48: 575-613.
31. Duan X, Sun H, Wang Y, Kang J, Wang S. N-doping-induced nonradical reaction on single-walled carbon nanotubes for catalytic phenol oxidation. ACS Catal. 2015; 5: 553-559.
32. Tan C, Gao N, Deng Y, Deng J, Zhou S, Li J, et al. Radical induced degradation of acetaminophen with Fe_3O_4 magnetic nanoparticles as heterogeneous activator of peroxymonosulfate. J Hazard Mater. 2014; 276: 452-460.
33. Fadaei S, Noorisepehr M, Pourzamani H, Salari M, Moradnia M, Darvishmotevalli M, et al. Heterogeneous activation of peroxymonosulfate with Fe_3O_4 magnetic nanoparticles for degradation of reactive black 5: Batch and column study. J Environ Chem Eng. 2021; 9: 105414.
34. Zhang Y, Xiangshi P, Tian J, Li F, Fan X, Ma L, et al. Synthesis of peroxymonosulfate composite catalyst (Fe^0/Fe_3O_4/biochar) using waterworks sludge and walnut shell for degrading methylene blue. J Environ Chem Eng. 2021; 9: 106856.
35. Zheng X, Niu X, Zhang D, Lv M, Ye X, Ma J, et al. Metal-based catalysts for persulfate and peroxymonosulfate activation in heterogeneous ways: A review. Chem Eng J. 2022; 429: 132323.
36. Pervez MN, He W, Zarra T, Naddeo V, Zhao Y. New sustainable approach for the production of Fe_3O_4/graphene oxide-activated persulfate system for dye removal in real wastewater. Water. 2020; 12: 733.
37. Khan MK, Farooq U, Noor H, Khan ME, Khan F, Ali SK, et al. Sustainable deep eutectic solvent-assisted synthesis of guar gum-derived carbon-supported $Sn_{0.96}Ni_{0.02}Co_{0.02}$/Al/Ce/Mo type-II oxide heterojunction for photo-Fenton-like degradation of chloramphenicol and photocatalytic CO_2 reduction. Sustain Mater Technol. 2025; 46: e01695.
38. Huda NU, Farooq U, Noor H, Khan ME, Ali W, Ali SK, et al. Interfacial design of $Sn_{0.96}Fe_{0.02}Ni_{0.02}O$/GGAC/γ-$Al_2O_3$/$CeO_2$/α-$MoO_3$ S-scheme heterojunction for PMS-activated photo-Fenton-like removal of phenol and hydrogen production. Environ Res. 2025; 285: 122703.
39. Farooq U, Noor H, Khan ME, Khan F, Alfifi F, Ali SK, et al. Dual-function oxygen-vacancy-rich $Zn_{0.98}Co_{0.02}O$/GGAC/γ-Al_2O_3/CeO_2/α-MoO_3 heterojunction with minimal metal leaching for PMS-driven 17α-ethinylestradiol degradation and CO_2-to-CH_4 conversion. J Ind Eng Chem. 2026; 154: 835-854.